Journal of Superconductivity and Novel Magnetism (2020) 33:397–406
https://doi.org/10.1007/s10948-019-05359-3

ORIGINAL PAPER

Magnetic, Structural, and Optical Properties of Gadolinium-Substituted $Co_{0.5}Ni_{0.5}Fe_2O_4$ Spinel Ferrite Nanostructures

M. F. Sarac[1]

Received: 26 August 2019 / Accepted: 14 November 2019 / Published online: 14 December 2019

Abstract

Gadolinium-substituted cobalt–nickel ferrite $Co_{0.5}Ni_{0.5}Gd_xFe_{2-x}O_4$ ($0 \leq x \leq 1.0$) nanostructures have been synthesized by hydrothermal approach which results more hydrophilic surface properties important for biomedical applications. Structural analysis by X-ray diffraction revealed the formation of a single-phase spinel ferrite for all samples and crystallite size is ranging from 13 to 28 nm. Lattice constant decreases with increasing Gd^{3+} ion concentration due to differences between ionic radii of Gd^{3+} and Fe^{3+}. Morphological analysis by scanning and transmission electron microscopy indicated the shape transformed from agglomerated particles into rod-shaped with increasing Gd content. Fourier transform infrared analysis also correlated the presence of the spinel ferrite structure. Optical band gap measurement implied that band gap decreases with increasing Gd content. In order to determine magnetic properties of cobalt–nickel spinel ferrite nanostructures, isothermal magnetization measurements have been obtained at 300 and 15 K using vibrating sample magnetometer. Magnetic properties are strongly depending on Gd substitution ratio, which alters the crystallite size, cation distribution, and exchange interactions between octahedral and tetrahedral sites of nanostructures. Saturation magnetizations decreased with increasing Gd substitution at both temperatures since cation distribution at different sites and large lattice distortion caused by Gd^{3+} ion substitution. Due to complex relations between the shape anisotropy, crystallite size, grain boundaries, secondary phases, and increasing Gd content observed in $Co_{0.5}Ni_{0.5}Gd_xFe_{2-x}O_4$ nanostructures, coercivity results in different magnetocrystalline anisotropy behavior.

Keywords Gadolinium substitution · Spinel ferrites · Magnetic property · Optical properties · Hydrothermal

1 Introduction

Spinel ferrites are significant class of ferrite materials due to their remarkable optical, magnetic, and electrical properties [1–5]. In the last decades, spinel ferrite nanomaterials have been attracted due to their wide range of applications such as read/write heads for high-speed digital tapes [6], magnetic sensors [7], permanent magnets [8], computer components [9], information storage systems [10], magnetic bulk cores [11], high-frequency transformers [12], biomedical applications [13], absorbing materials for microwave [14], and medical diagnostics [15]. Spinel ferrite nanoparticles are synthesized by various methods such as the auto-combustion method and flash combustion, citrate precursor, sol–gel, microwave-assisted, co-precipitation, and ceramic techniques [16, 17]. However, above synthesis methods generally give hydrophobic nanoparticles stabilized by nondegradable surfactants which have low magnetization [18]. Therefore, it is aimed to improve hydrophilic spinel ferrite nanostructures with controllable morphology including their size, shape, and composition with fast magnetic response. Because hydrothermal method refers to the synthesis by chemical reactions in nonaqueous solutions, it can drastically affect the reactivity and solubility of reactants which allows precise control of the morphology and high-crystallinity structures [18]. In addition, the magnetic properties of spinel ferrites can easily be modulated by alteration of chemical composition, annealing temperature and time, and distribution of cations between tetrahedral (A) and the octahedral (B) sites [19–21].

Spinel ferrites have general chemical formula of AB_2O_4 in which A occupies tetrahedral (A) interstitial sites, while B occupies octahedral (B) interstitial sites [2]. Saturation

---

✉ M. F. Sarac
fahrisarac@sdu.edu.tr

[1] Department of Mechanical Engineering, Faculty of Engineering, Suleyman Demirel University, 32260 Isparta, Turkey

magnetization values of spinel ferrites with rare earth material concentration can be interpreted by cation distribution and exchange interactions between tetrahedral (A) and octahedral (B) sites. Spinel ferrites belong to three types of interactions between A and B sub-lattices for magnetic ions such as A–A, B–B, and A–B super-exchange interactions. To the Neel's sub-lattice theory, A–B intra-sub-lattice interaction is stronger than the other two interactions since local strains and the super-exchange interaction between different ions dominantly affect the magnetic properties [22]. Among spinel ferrite family, cobalt ferrite ($CoFe_2O_4$) is one of the most important materials belonging to the inverse spinel group and exhibits high coercivity along with moderate magnetization, mechanical hardness, high chemical stability, and its cubic magnetocrystalline anisotropy [23–25]. Nickel ferrite ($NiFe_2O_4$) on the other hand is soft material with low coercivity and saturation magnetization at room temperature [26]. Both $CoFe_2O_4$ and $NiFe_2O_4$ have an inverse spinel structure in bulk form where all Me^{2+} occupy B-position (octahedral sites) and Fe^{3+} ions are equally distributed between tetrahedral and octahedral sites [27].

It has been shown that the addition of proper cations into the spinel structure causes the movement of cations among the accessible two lattice sites and this movement of cations directly affects magnetic properties of ferrites [28, 29]. Due to their high electrical resistivity, rare earth oxides are good electrical insulators, and this makes the rare earth oxides good candidates for substitution in spinel ferrites [30, 31]. Hence, doping of the proper chosen rare earth elements can promisingly modify the magnetic properties of spinel ferrites [32]. Many rare earth ions (like Gd^{3+}, Ho^{3+}, Y^{3+}, Nd^{3+}, Sm^{3+}, etc.) are substituted in the ferrites system, and a number of investigations have been done in this direction [33–35]. It was found that rare earth substitution causes structural disorder because of their larger ionic radius than that of both Fe and Co ions. Hence, very small amount of rare earth ion substitution changes the physical properties of ferrites [36–38]. The effect of Gd^{3+} ions substituted $NiFe_2O_4$ has already been reported by Dixit et al. [39], and they indicated that introduction of Gd^{3+} decreases the saturation magnetization and coercivity of $NiFe_2O_4$. Ahmad and Farid have investigated the effects of a small addition of Gd on the structure electric and magnetic properties of cobalt-based ferrites ($CoGd_xFe_{2-x}O_4$). They have reported that saturation magnetization increases while the coercivity decreases with increasing Gd content [40]. On the other hand, Peng et al. and Sodaee et al. reported that both saturation magnetization and coercivity of $CoFe_2O_4$ nanoparticles decrease by introducing Gd^{3+} ions [41, 42]. Additionally, many studies have reported the decrease in saturation magnetization but enhancements in coercivity values by Gd^{3+} ion substitution in $CoFe_2O_4$ nanoparticles [16, 35, 43].

Although Gd^{3+} substitution into cobalt and nickel ferrites is separately studied in the literature, to the best of our knowledge, synthesis and magnetic properties of Gd^{3+}-substituted $Co_{0.5}Ni_{0.5}Fe_{2-x}O_4$ (($0 \le x \le 1.0$) obtained by hydrothermal method have not been reported. Magnetic properties of Co–Ni ferrites can effectively enhance with Gd^{3+} substitution. Besides enhancing magnetic properties, using hydrothermal method may induce more hydrophilic surface properties that are extremely important in biomedical applications of these nanoparticles.

In this work, Gd-substituted cobalt–nickel spinel ferrites were synthesized by hydrothermal method, and their structural (XRD (X-ray diffraction diffractometer), EDS (energy-dispersive X-ray spectroscopy), FT-IR (Fourier transform infrared)), morphological (SEM (scanning electron microscopy) and TEM (transmission electron microscopy)), optical (% DR), and magnetic (VSM (vibrating sample magnetometer)) properties were investigated. The results propose that the Gd substitution in cobalt–nickel ferrite has considerable effect on the properties of obtained samples toward the progress of developing biomedical-based spinel materials.

2 Materials and Method

2.1 Materials

Nickel nitrate hexahydrate ($Ni(NO_3)_2.6H_2O$), cobalt (II) nitrate hexahydrate ($Co(NO_3)_2.6H_2O$) and iron (III) nitrate nonahydrate ($Fe(NO_3)_3.9H_2O$) were purchased from Kimetsan Company, Turkey, while gadolinium (III) nitrate hexahydrate ($Gd(NO_3)_3.6H_2O$) was received from Sigma-Aldrich and used as received.

2.2 Synthesis of Gd-Substituted $Co_{0.5}Ni_{0.5}Gd_xFe_{2-x}O_4$

The hydrothermal synthesis of Gd-substituted $Co_{0.5}Ni_{0.5}Fe_2O_4$ (($0 \le x \le 1.0$) nanostructures was prepared by using the stoichiometric ratio of iron, nickel, cobalt, and gadolinium nitrates which were dissolved in 50 mL deionized (DI) water with vigorous stirring. After treated with ultrasonic bath for 30 min, the prepared mixture was poured into a Teflon-lined vessel and transferred into a 100-mL stainless-steel Teflon autoclave. Hydrothermal reaction was taken place at 180 °C for 10 h. The obtained mixture was then washed three times with hot deionized water and centrifuged at 10.000 rpm for 10 min. Final solutions were dried at 80 °C for 5 h in Nuve FN400 dry heat oven.

2.3 Characterization

The morphology and composition analysis of $Co_{0.5}Ni_{0.5}Gd_xFe_{2-x}O_4$ ($0 \le x \le 1.0$) nanostructures were investigated by using the scanning electron microscopy (SEM) (FEI Quanta FEG 250) equipped with energy-dispersive X-ray spectroscopy (EDS) and transmission electron microscopy (TEM) (JEOL JEM-2100) techniques. X-ray diffraction diffractometer (XRD) (Bruker D8 Advance Twin Twin) with 40 mA, 30 kV, and Cu

Kα radiation (λ = 1.54059 Å) at room temperature over the 2θ range from 20° to 70° was used for the structural analysis. Fourier transform infrared (FT-IR) spectrum (Perkin Elmer BX FT-IR spectrophotometer) was recorded from 400 to 4000 cm^{-1} to observe the structure of formed chemical bonds. Characteristic of M-type hexaferrites was used for the detection of absorption bands. Ultraviolet-visible (UV-vis) diffuse reflectance (DR%, Agilent Cary 700 UMS) spectra were taken at 200- to 800-nm wavelength range for determining the optical band gap of the samples. The magnetic properties of all samples at room temperature (300 K) and 15 K were measured by vibrating sample magnetometer (VSM) (Lake Shore 7407 Series VSM) in a field of ±20 kOe.

3 Results and Discussion

3.1 XRD Analysis

Structural analysis of $Co_{0.5}Ni_{0.5}Gd_xFe_{2-x}O_4$ ($0 \leq x \leq 1.0$) nanostructures are performed by X-ray diffraction technique in Fig. 1. XRD measurements of samples were scanned in the 2θ range between 20° and 80°. The obtained diffraction peaks of $CoFe_2O_4$ and $NiFe_2O_4$ can be indexed to (220), (311), (222), (400), (422), (511), and (440) with most intense (311) reflection correlating the phase of polycrystalline cubic spinel structure. XRD reference patterns of $CoFe_2O_4$ (JCPDS: 22-1086) and $NiFe_2O_4$ (JCPDS: 86-2267) are very close together; thereby, it correlates the formation of each phase yielding $Co_{0.5}Ni_{0.5}Gd_xFe_{2-x}O_4$ nanostructure [26, 44, 45].

XRD measurements show that all samples have spinel structure. The lattice constant (a), unit cell volume (V), and crystallite size (D) taken from the broadening of the highest (311) peak by using Scherrer method with TOPAS refinement program were obtained as in Table 1. Nanocrystallities of all samples are found in the range of 13–28 nm. Due to increase in Gd^{3+} at cobalt–nickel ferrite structure, it leads to stress in crystal lattice and resulted on lattice parameter increase [45]. There is also a slight shift in the diffraction line which indicates that diffraction peaks are between $CoFe_2O_4$ and $NiFe_2O_4$. The intensity peak ratios of I_{220}/I_{222} and I_{511}/I_{222} decrease with an increase in Gd content, which are listed in Table 1. Furthermore, there is no trace of secondary phase for $x \leq 0.4$. This implies that the substitution of Gd^{3+} ions at low concentration is completely dissolved into the cobalt–nickel ferrite lattices. There are a small amount of orthoferrite phases $GdFeO_3$ (JCPDS: 74-1900) and Gd_2O_3 (JCPDS: 86-2477) appeared at concentrations where Gd content is higher than x = 0.4. Because ionic radius of Gd^{3+} ion (0.938 Å) is higher than that of Fe^{3+} (0.67 Å), there is a solubility limit for the replacement of Fe^{3+} into Gd^{3+} ions. This solubility limitation results in an excess substitution of Gd^{3+} ions to aggregate around the grain boundaries in the form of $GdFeO_3$ [16] and also separately to form Gd_2O_3 rod structures [46].

3.2 FT-IR Analysis

Fourier infrared spectroscopy (FT-IR) provides the exact configuration of ions in the structures. In Fig. 2, FT-IR analysis at room temperature from 400 to 1200 cm^{-1} shows that two absorption bands appeared on the structure of spinel ferrites due to vibrations of octahedral and tetrahedral metal–oxygen ions. Since the bond length varies for metal and oxygen atoms at both sites, it gives two different band positions. Both these absorption bands are characteristic for spinel ferrite structures [16]. The first frequency band, tetrahedral sites, was in the range of 594 to 605 cm^{-1}, while the second frequency which is octahedral sites was in the range of 417 to 420 cm^{-1}. When Gd substituted in the crystal structure, replacement of Fe^{3+} to Gd^{3+} decreases metal–oxygen bond length and resulted in

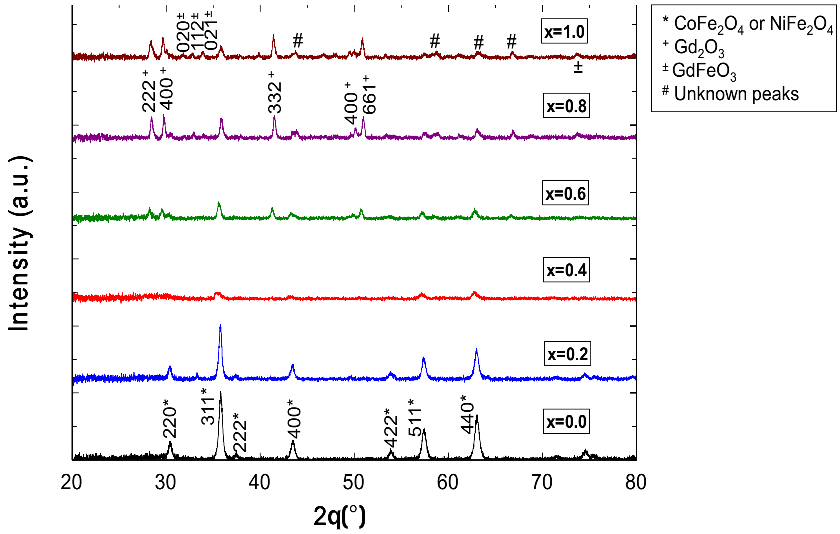

Fig. 1 X-ray diffraction (XRD) patterns of the $Co_{0.5}Ni_{0.5}Gd_xFe_{2-x}O_4$ ($0 \leq x \leq 1.0$) nanostructures

Table 1. Gd content and refined structural parameters (a is the lattice constant, V is the unit cell volume, and D_{XRD} is the crystallite size obtained from the broadening of the highest (311) peak by using Scherrer method) and the I_{220}/I_{222} and I_{511}/I_{222} ratios for the $Co_{0.5}Ni_{0.5}Gd_xFe_{2-x}O_4$ ($0 \leq x \leq 1.0$) nanostructures

x	a (Å)	$V(Å)^3$	D_{XRD}(nm)	I_{220}/I_{222}	I_{511}/I_{222}
0.0	8,345	581,137	20.97	4.043	7.425
0.2	8,352	582,601	26.79	2.219	6.176
0.4	8,361	584,486	13.73	1.670	3.749
0.6	8,373	587,007	23.11	1.455	3.327
0.8	8,389	590,378	28.22	0.998	0.880
1.0	8,406	593,975	23.04	0.830	0.789

octahedral sites to shift through higher frequency since the large radius of Gd^{3+} ions occupies octahedral sites. These higher-frequency absorptions are more apparent for higher concentration substitutions ($x > 0.4$). Furthermore, the intensity of absorption peaks decreases with increasing Gd addition due to the disordered state of the ferrite samples.

3.3 SEM and EDS Analysis

In order to get information for surface morphology, the FE-SEM images are taken for all samples. Different amounts of gadolinium-substituted $Co_{0.5}Ni_{0.5}Fe_2O_4$ nanostructures are shown in Fig. 3. It can be seen in Fig. 3 (a) that the none-gadolinium-substituted ferrite particles are agglomerated spherical-shaped structures. Increasing the gadolinium concentration on the ferrite structures results in a transformation from agglomerated clusters to rod-shaped structures and decreases in the grain size [46].

Energy-dispersive X-ray spectroscopy (EDS), which is in conjunction with FE-SEM, was used on elemental analysis for selected samples ($x = 0.2$ and $x = 0.6$) as shown in Fig. 4. The obtained results indicate the presence of Fe, Co, N, Gd, and O elements in the samples with no other impurities. The increase of the weight % of gadolinium from 15.42 to 18.44 confirms the increasing amount of gadolinium from $x = 0.2$ to $x = 0.6$.

3.4 TEM and SAED (Selected Area Electron Diffraction) Analysis

Figure 5 shows the HRTEM images for $x = 0.6$ of $Co_{0.5}Ni_{0.5}Gd_xFe_{2-x}O_4$ nanostructures. Porous and rod-shaped particles are observed along with mild to moderate agglomeration. Singular fine particles are about to 15-nm average size. The SAED patterns of the selected image are shown in the inset of the corresponding micrograph. The SAED pattern displays two distinct diffraction planes at one sample. Both crystal phase structures are crystalline phase of (a) cobalt ferrite spinel and Gd_2O_3 cubic structure. The lattice fringes of 0.45 and 0.19 nm were observed which correspond to (221) and (440) diffraction planes of cubic phase Gd_2O_3, while inter-fringe distance of 0.25 nm was observed which is attributed to {311} planar spaces of $CoFe_2O_4$ nanostructures.

3.5 Optical Analysis

Optical properties of $Co_{0.5}Ni_{0.5}Gd_xFe_{2-x}O_4$ nanostructures are analyzed by using diffuse reflectance UV-visible spectrophotometer ranging from 200 to 800 nm

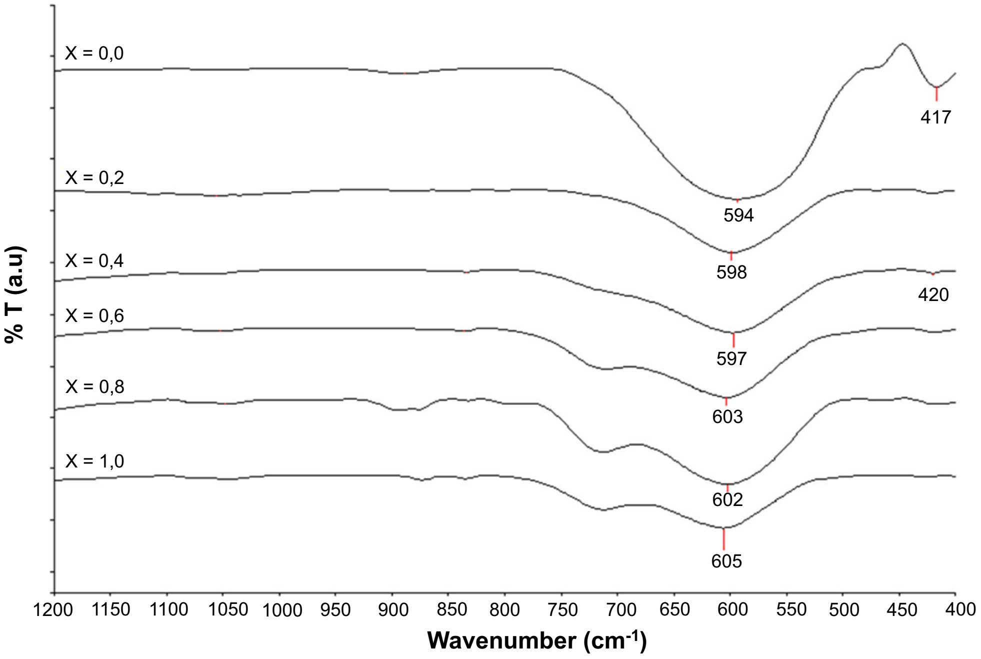

Fig. 2 FT-IR spectra of the $Co_{0.5}Ni_{0.5}Gd_xFe_{2-x}O_4$ ($0 \leq x \leq 1.0$) nanostructures

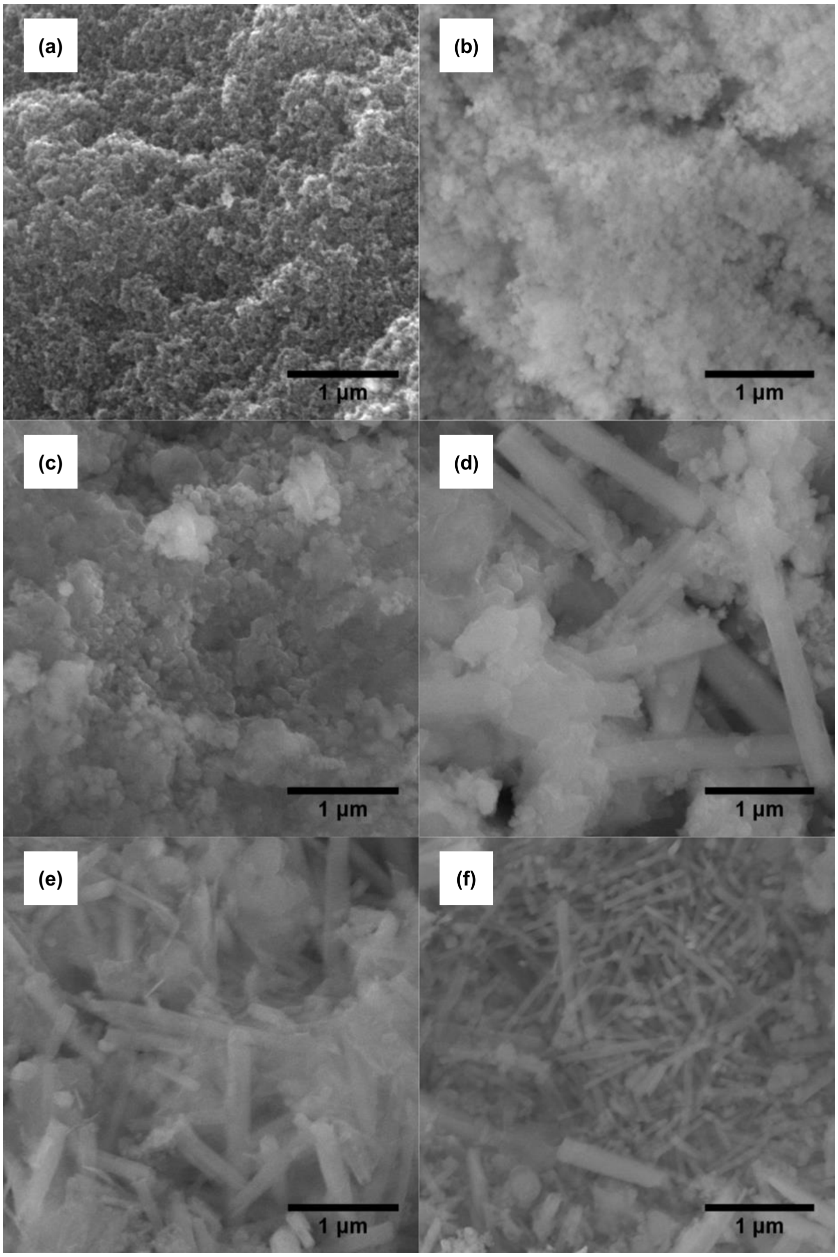

Fig. 3 Scanning electron microscope (SEM) images of $Co_{0.5}Ni_{0.5}Gd_xFe_{2-x}O_4$ ($0 \leq x \leq 1.0$) nanostructures for (a) x = 0, (b) x = 0.2, (c) x = 0.4, (d) x = 0.6, (e) x = 0.8, and (f) x = 1.0 at constant magnification

as shown in Fig. 6. The optical band gap energy (E_g) of each sample was calculated by using the Kubelka–Munk model [47]. At this model, a Tauc plot of $(\alpha h\nu)^{1/2}$ versus photon energy ($h\nu$) was drawn to obtain indirect band gap values [27].

The band gap values as determined from the graphs are 1.625, 1.598, 1.563, 1.55, 1.519, and 1.286 eV for x = 0, x = 0.2, x = 0.4, x = 0.6, x = 0.8, and x = 1.0, respectively, with Gd addition which leads to a weaker electrostatic interaction between occupied and unoccupied sites of $Co_{0.5}Ni_{0.5}Gd_xFe_{2-x}O_4$ nanostructures. The decrease in the band gap can be occurred with Gd addition by increasing the electron-hole recombination due to larger ionic radii of Gd^{3+} ions.

3.6 Magnetic Properties

Magnetic hysteresis loop measurements of $Co_{0.5}Ni_{0.5}Gd_xFe_{2-x}O_4$ at 15 and 300 K in the magnetic field range of ±20 kOe are shown in Fig. 7 a and b. Gd-substituted nickel–cobalt ferrite nanostructures show a ferrimagnetic nature at both temperatures. Saturation magnetization (M_s), remanent magnetization (M_r), magnetic anisotropy constant (K_α), ratio of remanence to saturation magnetization ($SQR = M_r/M_s$), coercivity (H_c), and magnetic moment (η_B) values have been obtained for 300 and 15 K and given in Table 2 and Table 3, respectively.

It can be noticed that the Gd substitution decreases the saturation and remanent magnetization values. The lowest saturation magnetization at 300 K (M_s = 3.98 emu/g) was

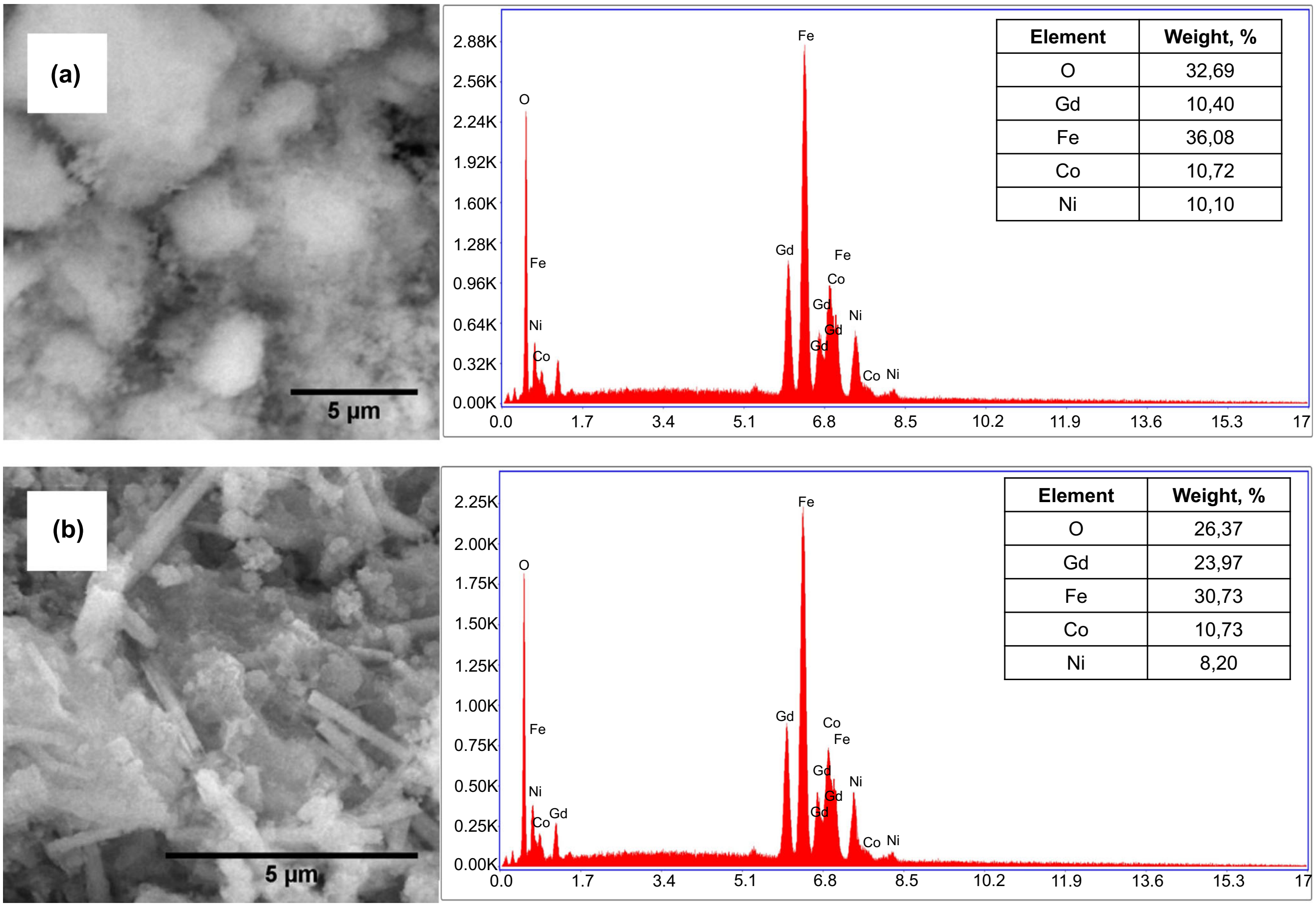

(a)

Element	Weight, %
O	32,69
Gd	10,40
Fe	36,08
Co	10,72
Ni	10,10

(b)

Element	Weight, %
O	26,37
Gd	23,97
Fe	30,73
Co	10,73
Ni	8,20

Fig. 4 SEM and their corresponding EDS spectrographs of the selected $Co_{0.5}Ni_{0.5}Gd_xFe_{2-x}O_4$ for (a) x = 0.4 and (b) x = 0.6 nanostructures

observed for x = 1.0 sample while Ms = 26.25 emu/g for 15 K. Due to the larger ionic radius of Gd^{3+}, Gd is prone to occupy octahedral sites in $Co_{0.5}Ni_{0.5}Gd_xFe_{2-x}O_4$ nanostructure with increasing Gd content, which tunes magnetic properties of samples [48]. In addition, Gd has the magnetic ordering temperature of $T_{Curie} = 292$ K and a lower spin-reorientation temperature T_{sr} = 225 K [49]. Therefore, Gd is in the paramagnetic state at 300 K. Substitution of Gd^{3+} ions in nickel–cobalt ferrite lattices is equal to the substitution of non-magnetic atoms at the octahedral sites (B), and hence, the magnetization of B sites is reduced. The total magnetization of nickel–cobalt ferrite is the difference between the magnetization of B and A sites [50, 51]. Consequently, the obtained saturation magnetization values of $Co_{0.5}Ni_{0.5}Gd_xFe_{2-x}O_4$

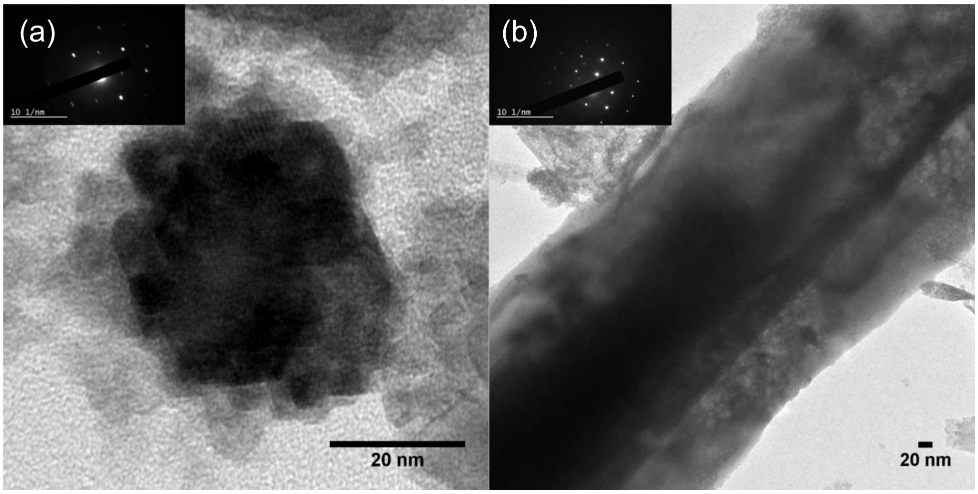

Fig. 5 Transmission electron microscopy (TEM) images and inset image as corresponding selected area electron diffraction (SAED) pattern of (a) cobalt–nickel spinel ferrite and (b) Gd_2O_3 nanostructures in the fraction of x = 0.6 at $Co_{0.5}Ni_{0.5}Gd_xFe_{2-x}O_4$ nanostructures

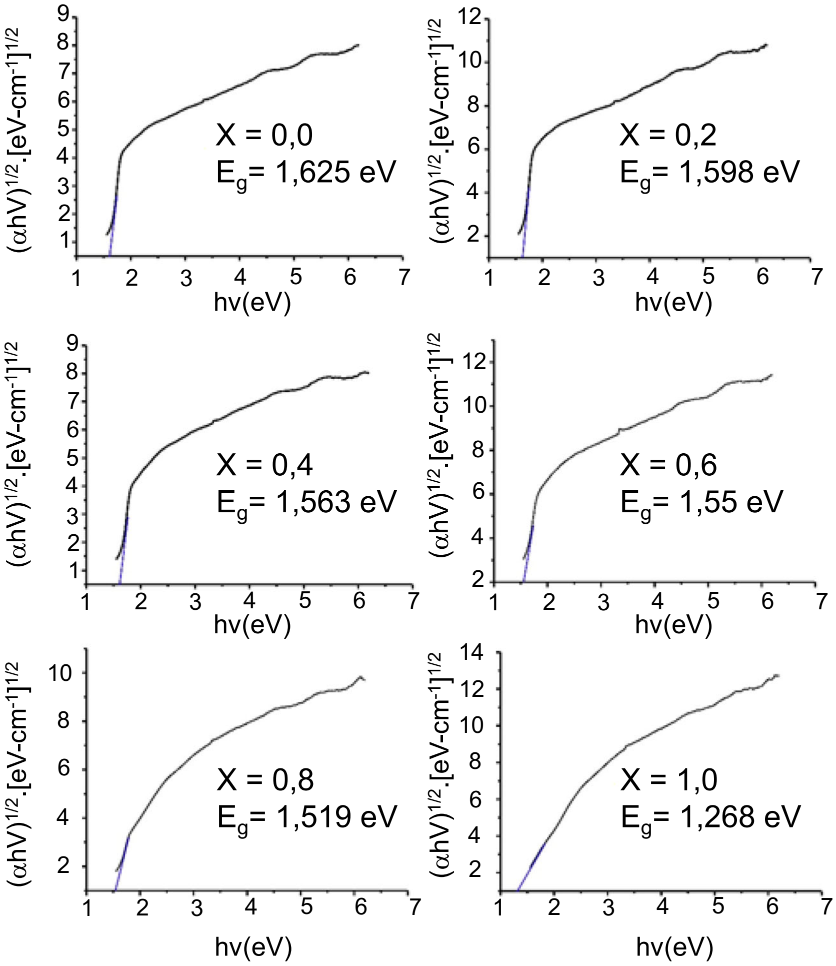

Fig. 6 $[\alpha h\nu]^{1/2}$ versus hν graphs of the $Co_{0.5}Ni_{0.5}Gd_xFe_{2-x}O_4$ ($0 \leq x \leq 1.0$) nanostructures

were smaller than $Co_{0.5}Ni_{0.5}Fe_2O_4$ inverse spinel ferrites due to its cation distribution and exchange interactions between octahedral (B) and tetrahedral (A) sites. In other words, gradually inserting Gd^{3+} ions into B sites distorted ferrimagnetic ordering and then deteriorated the strength of A–B superexchange interaction which decreases its saturation magnetization value from 42.47 emu/g to 3.98 emu/g.

Similar effect of Gd^{3+} substitution is also observed at 15 K. Saturation magnetization is reduced from 67.32 to 26.25 emu/g as Gd^{3+} substitution increases from 0 to 1.0. Compared to room temperature (300 K), M_s, M_r, and H_c values increase at 15 K. This occurrence caused by reduced thermal fluctuations of the magnetic moments, which is less effective in reducing the effects of magnetocrystalline anisotropy energy.

Similar to M_s and M_r, the variation in the values of coercivity is obtained from the magnetic hysteresis curves at both temperatures. Obtained coercive field values reveal that H_c first increases until x = 0.4 and then decreases with increasing Gd concentration. This observed variation in coercivity can be explained considering complex relations between the shape anisotropy, crystallite size, grain boundaries, and secondary phases. Depending on the crystallite size and shape observed from XRD and SEM, it tends to go through small crystallite size which reduces the crystallographic anisotropy of unit cell. The coercivity is inversely proportional to the crystallite size. Besides shape anisotropy, for higher rate of Gd^{3+} substitution (x > 0.4), secondary phases appeared. Presence of secondary phases around grain boundaries of spinel ferrites inhibits the domain wall displacement and results in an increase in coercivity [51]. On the other hand, increasing Gd^{3+} substitution results a shape transformation from agglomerated to rod-shaped particles which is introducing a shape anisotropy dependence on the measured coercivity. Since the nanoparticles are randomly distributed and there is no preferred orientation, the effect of shape anisotropy decreases the total coercivity.

Magnetic moment and magnetic anisotropy constant can be calculated from the following formulas for the relation with M_s and H_c as follows:

$$n_B = \frac{M_w M_s}{5585} \tag{1}$$

$$K_\alpha \approx \frac{M_s H_c}{5585} \tag{2}$$

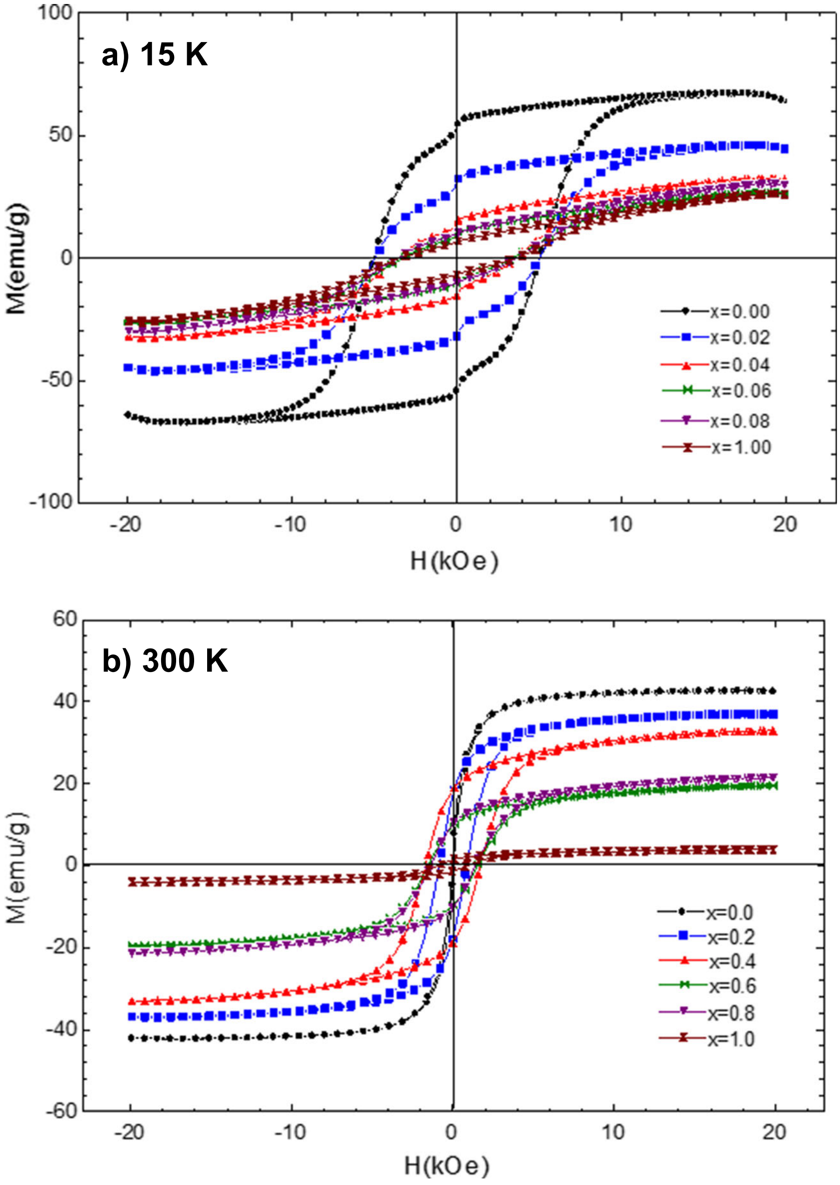

Fig. 7 Magnetic hysteresis curves for $Co_{0.5}Ni_{0.5}Gd_xFe_{2-x}O_4$ ($0 \leq x \leq 1.0$) nanostructures at (a) 15 K and (b) 300 K

Table 2. Magnetic parameters of the $Co_{0.5}Ni_{0.5}Gd_xFe_{2-x}O_4$ ($0 \leq x \leq 1.0$) nanostructures at 300 K temperature (x, molar ratio of Gd substitution; T, Kelvin in temperature; M_s, saturation magnetization; M_r, remanence magnetization; K_α, magnetic anisotropy constant; SQR, squareness ratio; H_c, coercivity; and η_B, magnetic moment)

x	M_s (emu/g)	M_r (emu/g)	SQR	H_c (Oe)	η_B (μ_B)	K_α (emf/cm^3)
0.0	42.47	2.65	0.062	36.79	1.783	0.28
0.2	37.09	17.40	0.469	863.26	1.692	5.732
0.4	32.99	18.57	0.563	1701.9	1.625	10.052
0.6	19.57	9.74	0.498	1525.1	1.035	5.345
0.8	18.63	8.84	0.474	1386	1.053	4.624
1.0	3.98	1.43	0.36	934.07	0.239	0.665

Table 3. Magnetic parameters of the $Co_{0.5}Ni_{0.5}Gd_xFe_{2-x}O_4$ ($0 \leq x \leq 1.0$) nanostructures at 15 K temperature (x, molar ratio of Gd substitution; T, Kelvin in temperature; M_s, saturation magnetization; M_r, remanence magnetization; K_α, magnetic anisotropy constant; SQR, squareness ratio; H_c, coercivity; and η_B, magnetic moment)

x	M_s (emu/g)	M_r (emu/g)	SQR	H_c (Oe)	η_B (μ_B)	K_α (emf/cm^3)
0.0	67.32	53.95	0.801	5027.5	2827	60,601
0.2	46.2	31.34	0.678	4989	2107	41,267
0.4	32.57	14.71	0.451	3611.4	1604	21,062
0.6	26.94	10.02	0.372	3329	1424	16,056
0.8	26.3	8.81	0.335	3606.7	1486	16,985
1.0	26.25	6.7	0.255	3503	1579	16,462

where M_w is the molecular weight of $Co_{0.5}Ni_{0.5}Gd_xFe_{2-x}O_4$ ($0 \leq x \leq 1.0$) nanostructures. The calculated $\mathcal{N}_B$ values and K_α of all samples at both temperatures are summarized in Table 2 and Table 3 as well.

The decrease in $\mathcal{N}_B$ values at both temperatures indicates a weakening of the super-exchange interaction with increasing Gd^{3+} content. Magnetic anisotropy constant is related to the coercive field. K_α gradually decreases except x = 0.8 with increasing Gd concentration resulting in the decrease in the magnetic anisotropy.

The squareness ratio (SQR: M_r/M_s) of each sample was calculated for both temperatures. It can be interpreted that SQR equal to or above 0.5 displayed that nanostructures behave as a single magnetic domain with uniaxial anisotropy, while below 0.5 represented multi-domain structure [51]. As seen in Table 2, the SQR at room temperature is around 0.563 for x = 0.4, while other samples ranging from 0.062 to 0.498 may include surface spin disorder effects [52].

4 Conclusions

Gadolinium-substituted Co–Ni ferrite powders have been synthesized by hydrothermal method. Substitution of Gd concentration made a drastic change in morphological, structural, optical, and magnetic properties of Co–Ni spinel ferrite structure. XRD and FT-IR results show the phase formation of cubic Co and Ni-spinel structure and lattice parameter decreased with increasing Gd^{3+} ion addition. SEM and TEM micrographs revealed that the shape of the powders transformed into rod-shaped structure with increasing Gd content. For x = 1, it is seen that the morphology is almost turned into rod-shaped structure. Optical properties of band gap energy decrease from 1.625 to 1.286 eV with increasing ionic radii of Gd^{3+} ions which lower the electrostatic interaction energy at octahedral sites of $Co_{0.5}Ni_{0.5}Gd_xFe_{2-x}O_4$ nanostructures. Cation distribution at different sites and large lattice distortion caused by Gd^{3+} ion substitution decrease the saturation magnetization at both (300 and 15 K) temperatures which also reduces the magnetization of the samples. Due to complex relations between the shape anisotropy, crystallite size, grain boundaries, secondary phases, and increasing Gd content, coercivity shows as either single or multi-domain uniaxial anisotropy.

References

1. Baykal, A., Kasapoglu, N., Koseoglu, Y., Basaran, A., Kavas, H., Toprak, M.: Microwave-induced combustion synthesis and characterization of $Ni_xCo_{1-x}Fe_2O_4$ nanocrystals (x = 0.0, 0.4, 0.6, 0.8, 1.0). Open Chem. J. **6**, 125–130 (2008)
2. Kasapoglu, N., Birsoz, B., Baykal, A., Koseoglu, Y., Toprak, M.: Synthesis and magnetic properties of octahedral ferrite $Ni_XCo_{1-x}Fe_2O_4$ nanocrystals. Open Chem. J. **5**, 570–580 (2007)
3. Deligoz, H., Baykal, A., Toprak, M.S., Tanriverdi, E.E., Durmus, Z.: Sozeri, H.; Synthesis, structural, magnetic and electrical properties of $Co_{1-x}Zn_xFe_2O_4$ (x = 0.0, 0.2) nanoparticles. Mater. Res. Bull. **48**, 646–654 (2013)
4. Ati, A.A., Othaman, Z., Samavati, A.: Influence of cobalt on structural and magnetic properties of nickel ferrite nanoparticles. J. Mol. Struct. **1052**, 177–182 (2013)
5. Ati, A.A., Othaman, Z., Samavati, A., Doust, F.Y.: Structural and magnetic properties of Co–Al substituted Ni ferrites synthesized by co-precipitation method. J. Mol. Struct. **1058**, 136–141 (2014)
6. Bharathi, K.K., Ramana, C.V.: Improved electrical and dielectric properties of La-doped Co ferrite. J. Mater. Res. **26**(4), 584–591 (2011)
7. Jain, S., Parashar, J., Kurchania, R.: Effect of magnetic field on terahertz generation via laser interaction with a carbon nanotube array. Int. Nano Lett. **3**, 5p (2013)
8. Thakur, A., Thakur, P., Hsu, J.-H.: Magnetic behaviour of $Ni_{0.4}Zn_{0.6}Co_{0.1}Fe_{1.9}O_4$ spinel nano-ferrite. J. Appl. Phys. **111**(7), 07A305 (2012)
9. Gul, I.H., Pervaiz, E.: Comparative study of $NiFe_{2-x}Al_xO_4$ ferrite nanoparticles synthesized by chemical co-precipitation and sol–gel combustion techniques. Mater. Res. Bull. **47**(6), 1353–1361 (2012)
10. Singhal, S., Singh, J., Barthwal, S.K., Chandra, K.: Preparation and characterization of nanosize nickel-substituted cobalt ferrites ($Co_{1-x}Ni_xFe_2O_4$). J. Solid State Chem. **178**(10), 3183–3189 (2005)
11. Mane, D.R., Birajdar, D.D., Patil, S., Shirsath, S.E., Kadam, R.H.: Redistribution of cations and enhancement in magnetic properties of sol–gel synthesized $Cu_{0.7-x}Co_xZn_{0.3}Fe_2O_4$ ($0 \leq x \leq 0.5$). J. Sol-Gel Sci. Technol. **58**(1), 70–79 (2010)
12. Abbas, Y.M., Mansour, S.A., Ibrahim, M.H., Ali, S.E.: Microstructure characterization and cation distribution of nanocrystalline cobalt ferrite. J. Magn. Magn. Mater. **323**(22), 2748–2756 (2011)
13. Hashim, M., Muddin, A., Kumar, S., Shirsath, S.E., Kotnala, R.K., Shah, J., Kumar, R.: Synthesis and characterizations of Ni^{2+} substituted cobalt ferrite nanoparticles. Mater. Chem. Phys. **139**(2-3), 364–374 (2013)
14. Muthuraman, K., Alagarsamy, S., Banu, M.A., Naidu, V.: Synthesis of Nano sized Ce-Co Doped Zinc Ferrite and their Permittivity and Hysteresis Studies. Int. J. Comput. Appl. **32**(3), 18–27 (2011)
15. Hankare, P.P., Sanadi, K.R., Garadkar, K.M., Patil, D.R., Mulla, I.S.: Synthesis and characterization of nickel substituted cobalt ferrite nanoparticles by sol–gel auto-combustion method. J. Alloys Compd. **553**, 383–388 (2013)
16. Murugesan, C., Chandrasekaran, G.: Impact of Gd^{3+} substitution on the structural, magnetic and electrical properties of cobalt ferrite nanoparticles. RSC Adv. **5**, 73714–73725 (2015)
17. Koseoglu, Y., Kurtulus, F., Kockar, H., Guler, H., Karaagac, O., Kazan, S., Aktas, B.: Magnetic Characterizations of Cobalt Oxide Nanoparticles. J. Supercond. Nov. Magn. **25**(8), 2783–2787 (2012)
18. Rafienia, M., Bighasm, A., Hassanzadeh-Tabrizi, S.A.: Solvothermal Synthesis Mgnetic Spinel Ferrites. J. Medical Signals Sens. **8**, 108–118 (2018)
19. Naeem, M., Shah, N.A., Gul, I.H., Maqsood, A.: Structural, electrical and magnetic characterization of Ni–Mg spinel ferrites. J. Alloys Compd. **487**, 739–743 (2009)
20. Devan, R.S., Kolekar, Y.D., Chougule, B.K.: Effect of cobalt substitution on the properties of nickel–copper ferrite. J. Phys. Condens. Matter. **18**, 9809 (2006)
21. Gul, I.H., Pervaiz, E.: Comparative study of $NiFe_{2-x}Al_xO_4$ ferrite nanoparticles synthesized by chemical co-precipitation and sol–gel combustion techniques. Mater. Res. Bull. **47**, 1353–1361 (2012)

22. Pachpinde, A.M., Langade, M.M., Lohar, K.S., Patange, S.M., Shirsath, S.E.: Impact of larger rare earth Pr^{3+} ions on the physical properties of chemically derived $Pr_xCoFe_{2-x}O_4$ nanoparticles. Chem. Phys. **429**, 20–26 (2014)
23. Yadav, R.S., Havlica, J., Masilko, J., Kalina, L., Wasserbauer, J., Hajdúchová, M., Enev, V., Kuřitka, I., Kožáková, Z.: Impact of Nd^{3+} in $CoFe_2O_4$ spinel ferrite nanoparticles on cation distribution, structural and magnetic properties. J. Magn. Magn. Mater. **399**, 109–117 (2016)
24. Karaagac, O., Bilir, B., Kockar, H.: Superparamagnetic cobalt ferrite nanoparticles: effect of temperature and base concentration. J. Supercond. Nov. Magn. **28**(3), 1021–1027 (2015)
25. Karaagac, O., Bilir Yildiz, B., Kockar, H.: The influence of synthesis parameters on one-step synthesized superparamagnetic cobalt ferrite nanoparticles with high saturation magnetization. J. Magn. Magn. Mater. **473**(1), 262–267 (2019)
26. Deraz, N.M., Abd-Elkader, O.H.: Processing and characterization of nano-magnetic $Co_{0.5}Ni_{0.5}Fe_2O_4$ system. J. Ind. Eng. Chem. **20**, 3251–3255 (2014)
27. Joshi, S., Kumar, M., Chhoker, S., Srivastava, G., Jewariya, M., Singh, V.N.: Structural, magnetic, dielectric and optical properties of nickel ferrite nanoparticles synthesized by co-precipitation method. J. Mol. Struct. **1076**, 55–62 (2014)
28. Almessiere, M.A., Slimani, Y., Guner, S., Nawaz, M., Baykal, A., Aldakheel, F., Sadaqat, A., Ercan, I.: Effect of Nb substitution on magneto-optical properties of $Co_{0.5}Mn_{0.5}Fe_2O_4$ nanoparticles. J. Mol. Struct. **1195**, 269–279 (2019)
29. Almessiere, M.A., Slimani, Y., Guner, S., Sertkol, M., Demir Korkmaz, A., Shirsath, S.E., Baykal, A.: Sonochemical synthesis and physical properties of $Co_{0.3}Ni_{0.5}Mn_{0.2}Eu_xFe_{2-x}O_4$ nano-spinel ferrites. Ultrason. Sonochem. **58**, 104654 (2019)
30. Almessiere, M.A., Slimani, Y., Guner, Nawaz, M., Baykal, A., Aldakheel, F., Akhtar, S., Ercan, I., Belenli, I., Ozcelik, B.: Magnetic and structural characterization of Nb^{3+}-substituted $CoFe_2O_4$ nanoparticles. Ceram. Int. **45**(7), 8222–8232 (2019)
31. Topkaya, R., Gungunes, H., Eryigit, S., Shirsath, S.E., Yildiz, A., Baykal, A.: Effect of bimetallic (Ni and Co) substitution on magnetic properties of $MnFe_2O_4$ nanoparticles. Ceram. Int. **42**(12), 13773–13782 (2016)
32. Baykal, A., Eryigit, S., Topkaya, R., Gungunes, H., Amir, M.D., Yildiz, A., Kurtan, U., Shirsath, S.E.: Magnetic properties and hyperfine interactions of $Co_{1-2x}Ni_xMn_xFe_2O_4$ nanoparticles. Ceram. Int. **43**, 4746–4752 (2017)
33. Amiri, S., Shokrollahi, H.: The role of cobalt ferrite magnetic nanoparticles in medical science. Mater. Sci. Eng. C. **33**, 1–8 (2013)
34. Bharathi, K.K., Ramana, C.V.: Improved electrical and dielectric properties of La-doped Co ferrite. J. Mater. Res. **26**, 584–591 (2011)
35. Pervaiz, E., Gul, I.H.: Low temperature synthesis and enhanced electrical properties by substitution of Al^{3+} and Cr^{3+} in Co–Ni nanoferrites. J. Magn. Magn. Mater. **343**, 194–202 (2013)
36. Dwevedi, S., Bharathi, K.K., Markandeyulu, G.: Magnetoreactance studies in rare earth-doped Ni ferrite. IEEE Trans. Magn. **45**, 4253–4256 (2009)
37. Sun, G.L., Li, J.B., Sun, J.J., Yang, X.Z.: The influences of Zn^{2+} and some rare-earth ions on the magnetic properties of nickel–zinc ferrites. J. Magn. Magn. Mater. **281**, 173–177 (2004)
38. Hemeda, O.M., Said, M.Z., Barakat, M.M.: Spectral and transport phenomena in Ni ferrite-substituted Gd_2O_3. J. Magn. Magn. Mater. **224**, 132–142 (2001)
39. Dixit, G., Singh, J.P., Srivastava, R.C., Agrawal, H.M.: Magnetic resonance study of Ce and Gd doped $NiFe_2O_4$ nanoparticles. J. Magn. Magn. Mater. **324**, 479–483 (2012)
40. Ahmad, I., Farid, M.T.: Characterization of cobalt based spinel ferrites with small substitution of gadolinium. World Appl. Sci. J. **19**, 464–469 (2012)
41. Peng, J., Hojamberdiev, M., Xu, Y., Cao, B., Wang, J., Wu, H.: Hydrothermal synthesis and magnetic properties of gadolinium-doped $CoFe_2O_4$ nanoparticles. J. Magn. Magn. Mater. **323**, 133–137 (2011)
42. Sodaee, T., Ghasemi, A., Razavi, R.S.: Microstructural characteristics and magnetic properties of gadolinium-substituted cobalt ferrite nanocrystals synthesized by hydrothermal processing. J. Clust. Sci. **27**, 1239–1251 (2016)
43. Puli, V.S., Adireddy, S., Ramana, C.V.: Chemical bonding and magnetic properties of gadolinium (Gd) substituted cobalt ferrite. J. Alloys Compd. **644**, 470–475 (2015)
44. Ortiz-Quinonez, J.-L., Pal, U., Villanueva, M.S.: Structural, magnetic, and catalytic evaluation of spinel Co, Ni, and Co−Ni ferrite nanoparticles fabricated by low-temperature solution combustion process. ACS Omega. **3**, 14986–15001 (2018)
45. Almessiere, M.A., Slimani, Y., Sertkol, M., Nawaz, M., Sadaqat, A., Baykal, A., Ercan, I., Ozcelik, B.: Effect of Nb^{3+} substitution on the structural, magnetic and optical properties of $Co_{0.5}Ni_{0.5}Fe_2O_4$ nanoparticles. Nanomaterials. **9**, 430–443 (2019)
46. Kang, J.G., Min, B.K., Sohn, Y.: Synthesis and characterization of $Gd(OH)_3$ and Gd_2O_3 nanorods. Ceram. Int. **41**, 1243–1248 (2015)
47. Vinosha, P.A., Das, S.J.: Investigation on the role of pH for the structural, optical and magnetic properties of cobalt ferrite nanoparticles and its effect on the photo-fenton activity, materials today: Proceedings, 5, 2, 8662-8671 (2018)
48. Kumar, G., Shah, J., Kotnala, R.K., Dhiman, P., Rani, R., Singh, V.P., Garg, G., Shirsath, S.E., Batoo, K.M., Singh, M.: Self-ignited synthesis of Mg–Gd–Mn nanoferrites and impact of cation distribution on the dielectric properties. Ceram. Int. **40**(9), 14509–14516 (2014)
49. Coey, J.M.D., Skumryev, V., Gallagher, K.: Is gadolinium really ferromagnetic? Nat. Brief Commun. **401**, 35–36 (1999)
50. Kumar, P., Sharma, S.K., Knobel, M., Chand, J., Singh, M.: Investigations of lanthanum doping on magnetic properties of nano cobalt ferrites. J. Electroceram. **27**, 51–55 (2011)
51. Khan, M.A.: Javid ur Rehman, M., Mahmood, K., Ali, I., Akhtar, M.N., Murtaza, G., Shakir, I., Warsi, M.F.: Impacts of Tb substitution at cobalt site on structural, morphological and magnetic properties of cobalt ferrites synthesized via double sintering method. Ceram. Int. **41**, 2286–2293 (2015)
52. Maaz, K., Mumtaz, A., Hasanain, S.K., Ceylan, A.: Synthesis and magnetic properties of cobalt ferrite ($CoFe_2O_4$) nanoparticles prepared by wet chemical route. J. Magn. Magn. Mater. **308**(2), 289–295 (2007)